EMI Characterization from GaN Power Amplifier Nonlinearity Test for 16-QAM 5G Communication

Hongyu DU [1], Fayu WAN [1], Vladimir MORDACHEV [2], Eugene SINKEVICH [2], Xiaohe CHEN [3], Blaise RAVELO [1]

[1] Nanjing University of Information Science & Technology (NUIST), 210044 Nanjing, Jiangsu, China
[2] Belarusian State University of Informatics and Radioelectronics, Minsk, Belarus
[3] China University of Petroleum, College of Information Science and Engineering, Beijing, China

{hongyu.du, fayu.wan, blaise.ravelo}@nuist.edu.cn, {mordachev, esinkevich}@bsuir.by, xchen@cup.edu.cn

Submitted July 2, 2024 / Accepted September 24, 2024 / Online first November 4, 2024

Abstract. *Today, the anywhere, anyhow and anytime application scenarios of 5G system force designer to challenge on electromagnetic interference (EMI) requirements. Despite the technological progress, relevant test techniques are necessary to minimize the future communication system EMI risk. In this paper, the EMI characterization from nonlinearity (NLT) of 5G system Gallium Nitride (GaN) power amplifier (PA) is studied. Firstly, the PA NLT is evaluated by 1-dB/3-dB/6-dB compression point and 3rd-order intermodulation distortion (IMD3). Then, a measurement platform is built based on vector signal generator and EMI receiver including digital modulation system. According to the adjacent channel leakage ratio (ACLR), error vector magnitude (EVM) and signal-to-noise ratio (SNR), the EMI characteristics of 3.5-GHz carrier signals modulated by 16-Quadrature Amplitude Modulation (16-QAM) distorted by the GaN PA NLT are discussed. Due to the GaN PA 3rd order intermodulation (IM3) product, the SNR degrades from 34.8 dB to 14.6 dB when the input signal power increases from –10 dBm to 6 dBm. The EMI effect is confirmed by significant signal distortion observed with 16-QAM constellation diagram. Research work is currently ongoing for extending the EMI test technique for 6G communication system.*

Keywords

EMI impact, nonlinear characterization, 5G communication, 16-QAM, signal distortion, signal-to-noise ratio (SNR)

1. Introduction

The today vision on wireless communication system evolves toward the spreading of 6G technologies [1]. However, the electromagnetic compatibility (EMC) design researchers have to overcome significant open problems before the maturity of 6G wireless transceiver (TxRx) [1]. Among the emphasized problems, appropriate solution must be developed against EMC and EMI challenges [2–4]. Remarkable EMC analyses of wireless systems were reported by estimation the signal-to-noise ratio [5], [6]. It was found that the nonlinear (NL) effects of TxRx active components as power amplifiers (PAs) constitute one of the main causes of radio frequency interference (RFI) [7–9]. For example, the out of band signal interference was detected due to amplitude-modulation effect [8]. An NL model of EMI-induced distortion phenomena was suggested with a circuit constituted by feedback CMOS operational amplifiers [9], [10]. The effect of high-power EMI from switching amplifier operating with digital modulated signal was investigated [11].

To deal with unintentional RFI issues in the communication systems, some tentative approaches notably intended to the EMI reduction were proposed by exploring spread spectrum technique [13] and pseudorandomized carrier frequency modulation [14]. A predictive approach of the impact of magnetic components was introduced for EMI suppression on the PA baseband [15]. Behind the EMI reduction approach, the mechanism can be understood more deeply with the consideration of NL distortions, in particular, of modulated signals [16]. A design methodology of low-distortion component was introduced [17]. However, the EMI effect was performed notably with analysis, modelling, computation and estimations of high-frequency harmonics distortion from transmitter (Tx) amplifier [18–22]. An innovative approach of intermodulation distortion (IMD) estimation is developed with RF component nonlinearities (NLTs) [23]. An analysis and design of third-order intermodulation (IM3) of a receiver (Rx) function is proposed [24].

However, due to real-world complexity and modeling limitations, there is a need for more innovative characterization methods for nonlinear analysis. For this reason, more innovative characteristic approach for NL analysis is necessary for example by taking into account the interaction between component and system [25]. So far, the EMI-induced distortion remains a hot topic in the RF and communication engineering [26]. Therefore, the EMC design researchers are constantly looking for relevant prediction methods of EMI effects cause by the amplifier NLT [27]. An EMI virtual testing of electronic devices was developed according to the EMC requirements [28]. Despite the accomplished experimental techniques [29], further improvement of EMC pre-

DOI: 10.13164/re.2024.0669

compliance testing's notably to the 5G and 6G TxRx components is ongoing.

The main contributions of the present research work are:

- EMI characterization of a self-developed microwave gallium nitride (GaN) power amplifier NLT.
- The developed test methodology includes P1dB and IMD3 evaluation using 16-QAM communication signals. The power amplifier IMD3 is characterized by a dual-frequency test system [30], [31].
- The EMI characterization technique is linked qualitatively and quantitatively through the qualitative and quantitative links established between the power amplifier's IMD3 and the error vector magnitude (EVM).

The paper is organized in three main sections. Section 2 describes the device under test (DUT) which is a GaN high PA (HPA) and the NL characterization test plan. The single-carrier NL test including the PA gain, 1dB compression point (P1dB), 3dB compression point (P3dB), 6dB compression point (P6dB) efficiency and IMD3 characterization is explored. Section 3 investigates on the EMI experimental analysis due to the PA NLT based on EVM and signal-to-noise ratio (SNR) of 5G communication multi-band adjacent channels with 16-QAM signals. Then, Section 4 is the final conclusion.

2. Single-Carrier NL Test Characterization of GaN HPA DUT

After the PA DUT and employed instruments description, the performed characterization is carried-out at the test frequency $f_0 = 3.5$ GHz with stored corresponding data results available in [42] and examined in the present section.

2.1 Description of GaN PA DUT and Used Instruments

The present subsection defines the specifications of the DUT consisted of Gallium Arsenide (GaAs) driver and GaN main amplifiers explored for the NL and EMI characterization with 5G communication signals. The perspective view and schematic diagram of the GaN HPA DUT are shown in Fig. 1(a) and (b), respectively.

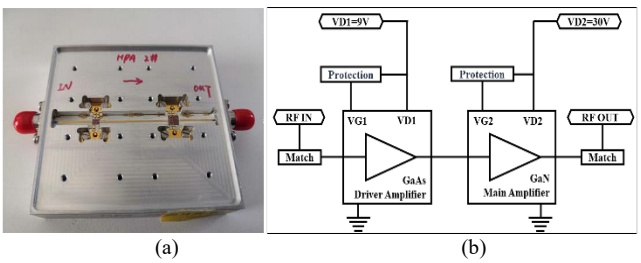

(a) (b)

Fig. 1. (a) Photograph and (b) schematic diagram of the GaN HPA DUT.

Description	Parameter	Value
Size	Length×Width×Heigth	(70 ×60 ×40) mm
Gate DC bias (quiescent current)	Power	+9 V/330 mA
	Dynamic currents	0.4 A–0.6 A
Drain DC bias (quiescent current)	Power	+30 V/670 mA
	Dynamic currents	1.2 A–1.8 A
Small-signal gain typical value	G_{small}	42 dB
Power gain typical value	G_{large}	32 dB
Saturated output power	$P_{out,sat}$ @ P_{in} = 10 dBm	41 dBm
Maximum allowed input power	$P_{in,A}$	14 dBm
Input/output connectors	SMA	3.5 mm (F)
Bandwidth	-	2–6 GHz

Tab. 1. Specifications of the GAN PA DUT.

For the present research work, the PA DUT:

- Was fabricated by using a 250 nm GaN High-electron-mobility transistor (HEMT) in monolithic microwave integrated circuit (MMIC) process;
- Was packaged and implemented in hybrid microstrip board on Rogers4350B substrate as photographed in Fig. 1(a);
- Is a typical broadband high PA chip having 3.88 mm × 3.49 mm × 0.1 mm physical size that is grounded through a metal via hole on the back;
- Is a two-stage amplification lumped circuit with schematic diagram depicted in Fig. 1(b);
- Is supplied by VD_1 from the drain power port through the voltage conversion circuit which protects to generate the gate voltage VG_1, for the first stage block constituted by GaAs PA circuit;
- Is supplied by VD_2 from the drain power port of the second stage and through the protection circuit to generate the gate voltage of the GaN PA circuit;
- And both GaAS and GaN PA circuits are designed with protection circuits, and there is no requirement for the power-up timing of the drain of both during power-up.

The microwave HPA implemented in GaN technology was designed and manufactured in order to operate with specifications indicated in Tab. 1.

The DUT operates as a broadband HPA within a microwave frequency band.

The DUT is essentially specified by its direct current (DC) bias, dynamic currents, small-signal gain, power gain, saturated output power and maximum allowed input power. The specifications of instruments employed during the test are defined in the following subsection.

2.2 Instrument Test Specifications

The experiment purpose is the PA NLT assessment by means of RF output measurement with a spectrometer. The measured NLT result is recorded synchronously in order to determine the PA input-output characteristics and to calculate the PA gain. The test was performed by adjusting the

vector signal generator (VSG) parameters to change the PA RF input. The considered instruments used for the GaN HPA test under investigation includes a VSG, attenuator, spectrometer and several coaxial cables with adapter whose specifications are described as follows:

- The VSG model used in the test is E8267D Agilent reference which can generate signals from 250 kHz to 44 GHz and supports both analog and IQ modulation.
- The E4447A Agilent spectrometer presents up to 80 MHz analysis bandwidth, +/–0.19 dB absolute amplitude accuracy, –168 dBm Displayed Average Noise Level (DANL), –118 dBc/Hz phase noise at 10 kHz bias, and 81 dBW-Code Division Multiple Access (CDMA) ACLR dynamic range, it supports measurements of complex RF and microwave signals from 3 Hz to 42.98 GHz.
- And the 2.92TS20-20-40 attenuator was used with 20-dB attenuation, DC to 40 GHz frequency range and a 20 W power rating.

In on-state, the PA is fed by two different DC power supplies (PSs) with 9-VDC for the Gallium Arsenide (GaAs) driver amplifier and 30-VDC. The first voltage source referenced by E3648A Agilent DC 50-W PS provides DC power up to voltage-current (5 V, 9 A) and (20 V, 2.5 A). The other source referenced by Agilent E3632A DC PS, rated at 120 W, provides a maximum output of voltage-current (15 V, 7 A) and (30 V, 4 A).

2.3 PA NL Experimental Setup

The experimentation was performed by paying attention on the attenuation and loss affecting the measured PA output signal power.

Before the test, the vector network analyzer (VNA) was connected to the attenuator used to avoid its saturation through coaxial lines. The measurement of PA input and output signal powers takes into account the coaxial line loss at both ends and the output attenuation. The block diagram dedicated to the attenuation measurement of the considered attenuator and PA RF coaxial line loss is shown in Fig. 2(a). The attenuator connected to the long and short cables specified within different input power ranges as addressed in Tab. 2 has a slight difference in attenuation at different input powers.

In order to ensure the overall test accuracy, the induced losses are removed after the final test. The block diagram of the GaN PA input-output NL test is drawn in Fig. 2(b). The single-carrier signal NL test experimental setup is illustrated by the view of Fig. 2(c).

Input power (dBm)	–30 to –12	–10 to –2	0 to 8	10
Long coaxial cable (dB)	0.97	0.96	0.96	1
Attenuator + short coaxial cable (dB)	19.88	19.87	19.86	19.87

Tab. 2. Specifications of employed coaxial cables and attenuator.

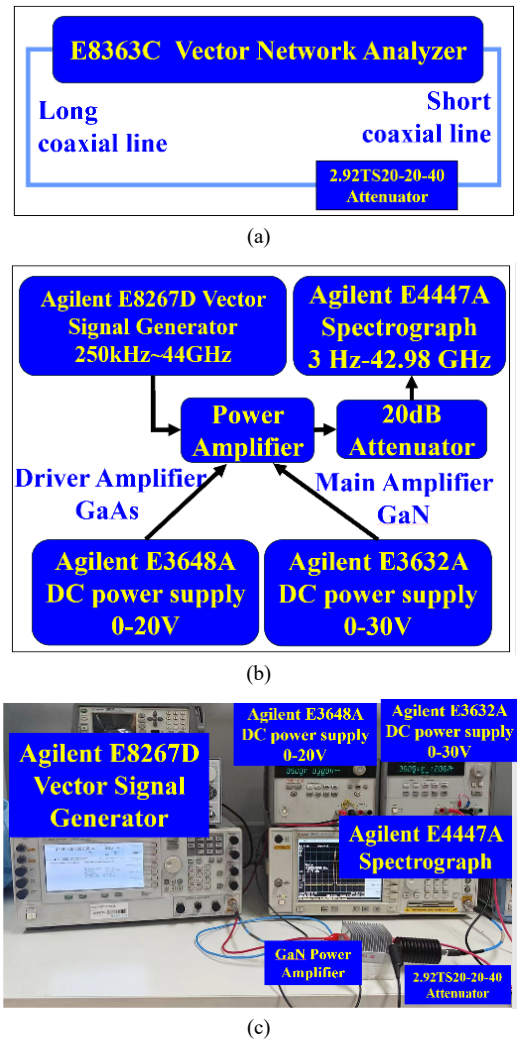

Fig. 2. (a) Attenuation measurement diagram including interconnection coaxial lines, (b) test block diagram and (c) test setup of PA input-output power.

The NL characteristics obtained from the measured PA input-output data are examined in the next subsection.

2.4 Discussion on PA RF Input-Output Results

The RF characteristics of the power amplifier were tested within the passband (2–6 GHz) and spanning 40 MHz by injecting signals with powers ranging from –30 dBm to 10 dBm into the PA and measuring them at 2 dBm intervals.

The first step in wireless single-carrier testing focuses on evaluating the Input-Output characteristics of the PA shown in Fig. 3(a) over the passband range.

When the input signal power P_{in} is varied from $P_{in,min} = -30$ dBm $\leq P_{in} \leq -10$ dBm, the PA operates in the linear region. However, for $P_{in} > -10$ dBm, the PA input and output characteristic slope becomes been less than 1. The behavior indicates when from $P_{in} > -10$ dBm, the DUT GaN PA operates in the NL amplification area. Figure 3(b) shows the PA gain and Figure 3(c) shows efficiency with the input-output power characteristic.

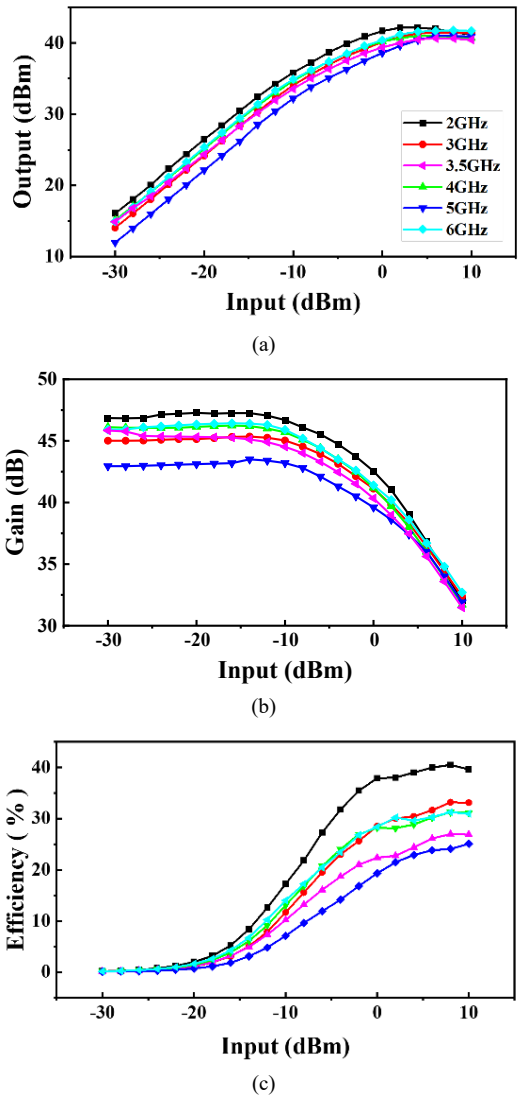

Fig. 3. (a) PA input-output characteristic, (b) plot of gain and (c) efficiency versus output power.

In this case, the efficiency is defined by the ratio of the PA output RF to DC power. The efficiency of a power amplifier indicates how efficiently it converts energy from DC to RF. From Fig. 3, the linear gain of the power amplifier is 45.5 dB, the saturation power reaches 40.5 dBm, and the saturation efficiency reaches 26.9% when the operating frequency is $f_0 = 3.5$ GHz because this frequency belongs to 5G communication in China. We would like to underline that 5 GHz response shown in Fig. 3 looks far away from {2, 3, 3.5, 4, 6} GHz because globally of parasitic effects related to the interface mismatching and also the electrical interconnect probable resonance frequencies. During the test at a certain frequency, as the input power continues to change, the drain current will also change, by waiting for the DC PS E3632A display to stabilize, and record the drain current values.

2.5 IMD3 Characterization Test Results with Two-Tone Signal

The VSG operation mode was configured to provide with two-tone input signal with carriers f_1 and f_2. During the NL test, the VSG output was linearly increased from $P_{in,min} = -20$ dBm $\leq P_{in} \leq P_{in,max} = 10$ dBm until the IMD3 was observed by the spectrometer. In this study case, the expected theoretical and measured spectral power frequencies indicated in Tab. 3 was recorded by using spectrometer marker. The HPA measured IMD3 from the test data is displayed in Fig. 4(a).

The IMD3 distortion is defined by the difference between the fundamental components, f_1 and f_2, and the IM3 components, $2f_1 - f_2$ and $2f_2 - f_1$. By increasing the PA input power from $P_{in,min}$ during the experimentation, the NL region appears. The IMD3 increases with the rate greater than the fundamental component rate increase.

Thus, it can be seen from Fig. 4(a) that IMD3 decreases as the power of the input signal gradually increases. Especially in the nonlinear region, IMD3 remains low, which is mainly due to the fact that the IM3 component increases

Type	Parameter	Theory	Measurement
Fundamental	$\lvert f_1 - f_0 \rvert$	5 MHz	5.19 MHz
	$\lvert f_2 - f_0 \rvert$	5 MHz	5.06 MHz
IMD3	$\lvert (2f_1 - f_2) - f_0 \rvert$	15 MHz	15.19 MHz
	$\lvert (2f_2 - f_1) - f_0 \rvert$	15 MHz	15.04 MHz

Tab. 3. Calculated vs measured fundamental & harmonic frequencies.

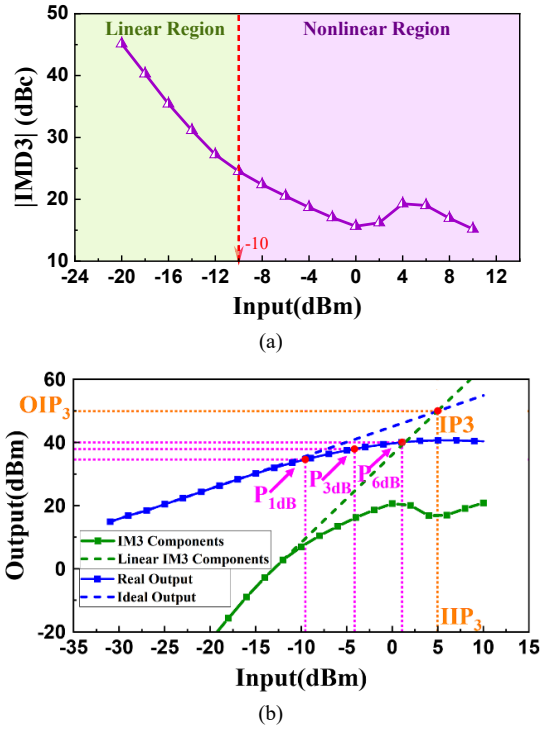

Fig. 4. (a) IMD3 and (b) NL characteristics vs P_{in}.

Designation	Parameter	Measured value
Linear gain	G	45.5 dB
Power saturation	P_{sat}	40.5 dBm
Saturation power	η	26.9%
1-dB compression point	P_{1dB}	34.6 dBm
3-dB compression point	P_{3dB}	37.9 dBm
6-dB compression point	P_{6dB}	40.1 dBm
3rd order intercept point	(IP3, OP3)	(5 dBm, 49.78 dBm)

Tab. 4. NL characteristics of the GaN PA DUT.

faster in this region. However, when the PA enters the saturated operating region, due to the clipping effect, some of the cross-modulation products are weakened, and the IMD3 can pick up. The NL characteristics are plotted by Fig. 4(b).

After analysis of this experimental result, the linear gain $G = \mathrm{dB}(P_{out}/P_{in})$, saturation power P_{sat}, saturation efficiency η, P_{1dB}, P_{3dB}, P_{6dB} and the 3rd order intercept point (IP3) of GaN HPA are quantified. The DUT empirical NL characteristics are addressed by Tab. 4. More importantly, the main parameter susceptible to play on the Tx EMI is the third-order cross-modulation rejection which is evaluated below $IMD3_{min} = 24.5$ dB in the NL region. It is keen to quantify the 5G TxRx communication performance degradation due to the unwanted EMI caused by the GaN PA NL effect.

3. EMI Impact Due to the GaN HPA NLT on the 5G TxRx Communication

The GaN HPA NLT impact on the performance of 5G communication performance is investigated in this section. The EMI characteristic is assessed via ACLR, EVM and SNR with respect to the 3GPP EMC compliance standard using 16-QAM communication signal having carrier frequency f_0 with stored data results available in [42].

3.1 Test Instrument and EMI Platform Test Description

The experimental study revealing the EMI due to the GaN HPA NLT is examined in this section by using VSG and signal analyzer (SA) instrument. The EMI characterization under investigation is based on the use of Qingling Technology QL6711 vector signal (VS) TxRx analyzer photographed in Fig. 5(a). Carrier single wave signals with a center frequency of 3.5 GHz, power of –10 dBm~8 dBm, and code rate of 1 Msps were generated using the MSG2000A, respectively, and demodulated by Signal Analyzer after 16-QAM modulation, and then the demodulated signal parameters were analyzed. The TxRx VSA was monitored by MSG2000A carrier signal compilation, Figure 5(b) shows the compiler software interface. As shown in Fig. 5(b), the signal compilation software can display a series of information such as constellation diagram, eye diagram, power spectrum in terms of EVM of the demodulated signal.

This software's analysis enables to monitor the modulation/demodulation experiments with 16-QAM 5G communication signals with respect to 3GPP standard. The synoptic of the EMI experimentation test setup is illustrated by Fig. 6(a). The QL6711 VS provides different output signals with carrier frequencies f_0 and amplitude from minimum –10 dBm to maximum 6 dBm injected to the HPA. In this case, the input signal is injected to the QL6711 SA modulation module from its RF input port. Then, the EMI results correspond to the modulated EVM and ACPR spectrum of the input and output signals recorded after 16-QAM modulation. The overview of the performed EMI characterization platform is photographed in Fig. 6(b). The EMI test operation mode with respect to 5G communication is described as:

- After compiling the configuration file from the MSG2000A carrier signal, it was imported into the SA software, and the modulation mode was set to 16-QAM to test the communication before and after the system was connected to the PA.
- The initial signal power is –10 dBm, the step is 2 dBm, and the cut-off power is 8 dBm. Set the SA to observe the information such as signal type, resolution bandwidth, span width, reference level, etc.
- Then, in the final process, observe the changes of the SA constellation diagram, spectrum, etc., and obtain the experimented data.

Figure 7 shows the ACLR monitored by the experimental platform. Figures 7(a) and (b) show the ACLR at the input of –10 dBm and 0 dBm signals, respectively, and it can be seen that the power of the latter's neighboring channel is significantly higher than that of the former, which is precisely due to the nonlinearity of the PA.

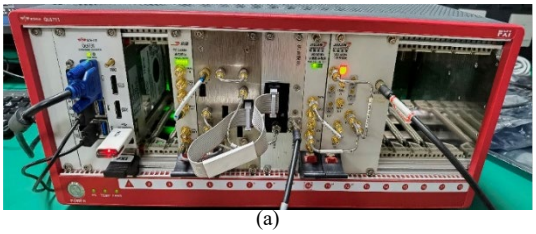

(a)

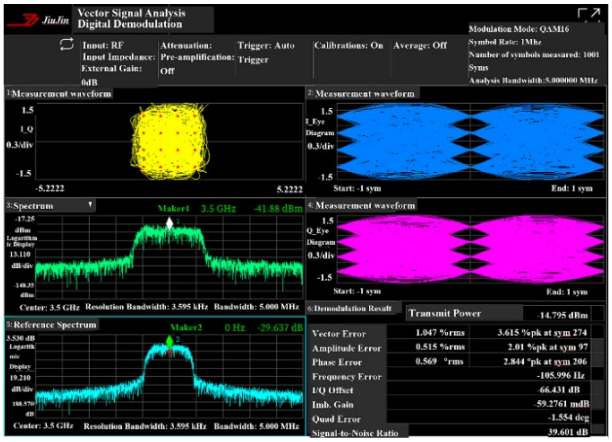

(b)

Fig. 5. (a) QL6711 TxRx VSA; (b) Screenshot of JiuJin vector signal analysis digital demodulation.

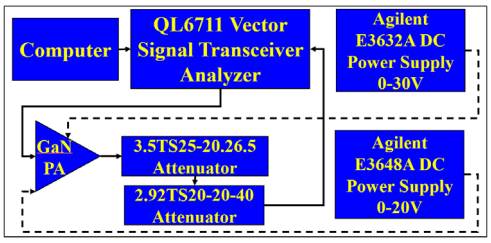

(a)

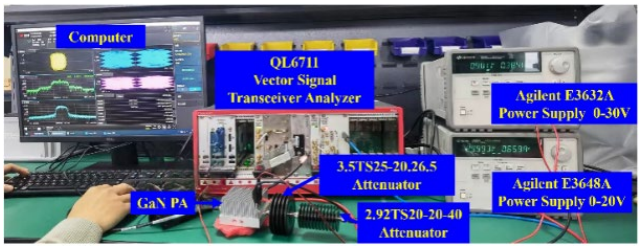

(b)

Fig. 6. (a) Synoptic diagram with respect to 3GPP EMC compliance standard and (b) photo of 5G communication EMI test platform.

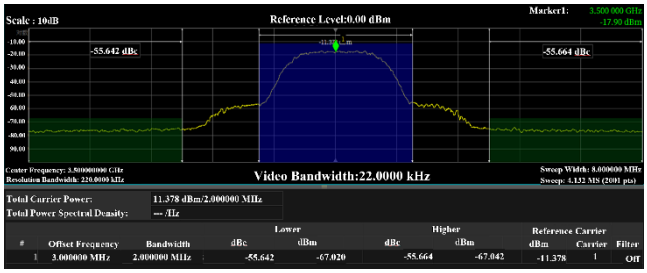

(a)

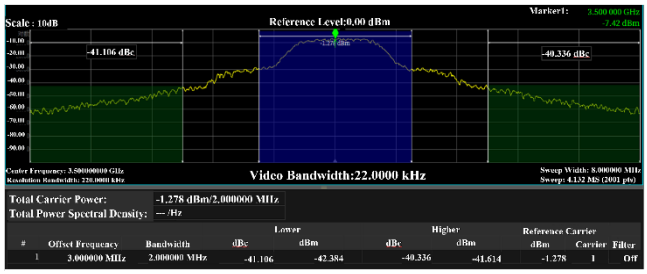

(b)

Fig. 7. ACLR with f_0-carrier 16-QAM modulation communication signal with (a) $P_{in} = -10$ dBm and (b) $P_{in} = 0$ dBm.

3.2 EMI Influence on Tx Power

The EMI experiment includes the GaN HPA NLT effect on the 16-QAM communication quality of 5G TxRx. The PA NLT influence on the communication system Tx power was measured by using FSW85 SA to modulate and demodulate the single-carrier signal with center frequency f_0 and 1-Msps bit rate. The 16-QAM test Tx power is shown in Fig. 8.

From Fig. 8, it can be seen that the communication system Tx power exhibits characteristics that match the amplifier nonlinearities derived in Sec. 2.5 (Fig. 4(b)). The Loaded Amplifier Mode (LAM) operates from –10 dBm, the signal starts to be amplified by the NL and transmits a signal power greater than that of the Direct Connection Mode (DCM) at $P_{in} < 0$ dBm, while the PA reaches saturation at $P_{in} = 4$ dBm.

3.3 EMI Impact on 5G TxRx Communication ACLR

In this case of study, a single-carrier signal f_0, input power of –10 dBm~8 dBm, and code rate of 1-Msps was generated using the MSG2000A. The ACLR performance of the tested signal plotted in Fig. 9(a) was observed by the SA after 16-QAM modulation without and with PA DUT, demonstrating the signal leakage below and above the neighboring channels on both sides of the main channel. Table 5 shows the total carrier and neighboring channel power of TxRx communication under 16-QAM modulation after DCM and with PA by considering different P_{in}.

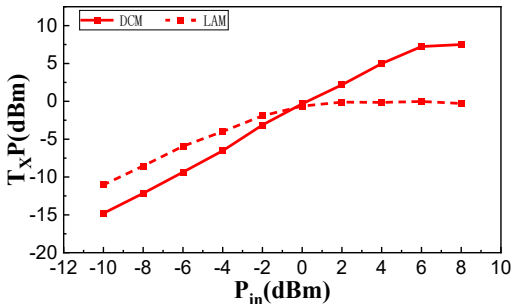

Fig. 8. Tx power with 16-QAM modulation.

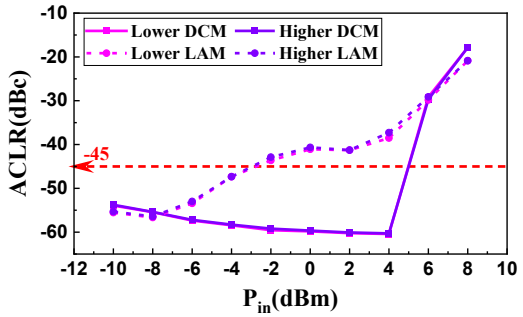

(a)

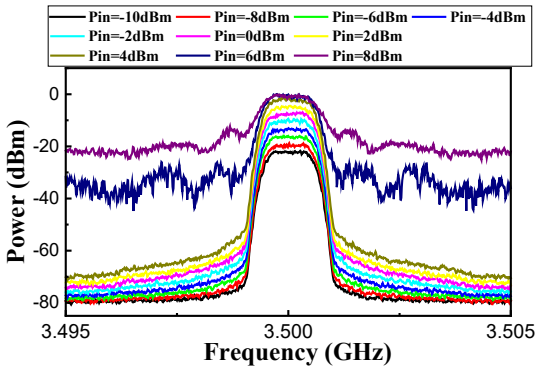

(b)

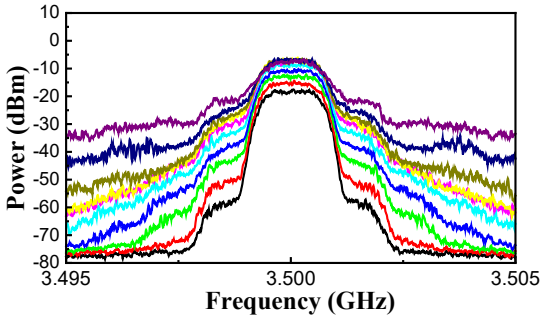

(c)

Fig. 9. (a) ACLR 16-QAM modulation @ f_0, and spectrum of (b) DCM and (c) LAM.

Modulation	Input (dBm)	DCM (dBm)	LAM (dBm)
Total carrier	–10	15.78	18.38
	–4	7.25	11.31
	2	1.22	7.17
	6	5.99	6.74
Neighborhood	–10	69.71	67.53
	–4	65.68	51.89
	2	59.01	42.09
	6	23.17	30.46

Tab. 5. Carrier and neighbor power (in dBm) in 16-QAM modulation TxRx communication with f_0-carrier.

P_{in}(dBm)	IMD3 (dBc)	EVM_{LAM} (%)	SNR_{LAM} (dB)
–10	24.57	1.65	34.18
–8	22.34	2.78	30.27
–6	20.57	4.95	25.60
–4	18.68	6.82	22.86
–2	17.03	9.38	20.07
0	15.59	12.58	17.52
2	16.2	15.07	15.43
4	19.26	16.79	14.43

Tab. 6. EVM and SNR with 16-QAM modulation.

From the PA input and output characteristics, it can be seen that the amplifier enters the NL region at $P_{in} = -10$ dBm, at which time the IM3 component has already appeared, and as the input signal rises, the gain gradually decreases, the suppression of the IM3 component becomes weaker, and the communication signal begins to show deterioration phenomena. From the comparative analysis of Fig. 9(b) and Fig. 9(c), it can be seen that the LAM has a significant deterioration in the ACLR at various input powers compared to the DCM. It can literally be emphasized that the LAM no longer meets the communication standard when $P_{in} > -3$ dBm. Figure 9(c) shows the signal spectrum at different input powers. In the DCM, when $P_{in} \leq 4$ dBm, the neighbor-channel suppression ratio is large. Nevertheless, when $P_{in} \geq 6$ dBm, the neighbor-channel suppression ratio decreases sharply. In the LAM, the neighboring channel power starts to show an increase at the beginning –10 dBm.

Hence, as P_{in} rises, the neighboring channel power rises with it, and when $P_{in} > 0$ dBm, the total power of the carrier rises very slowly, while the neighboring channel power rises faster. This phenomenon shows that the PA NLT will reduce the 5G TxRx communication ACLR.

3.4 Analysis of EVM and SNR

The signal modulation accuracy reflects the 5G communication system overall performance, which integrates the effects of I/Q imbalance, NL distortion, phase noise, flatness and other factors on the signal quality. In the modulation accuracy test, the EVM deterioration degree of a single-carrier signal by a PA is measured. A single-carrier signal f_0, a power ranging from –10 dBm to 8 dBm, and a code rate of 1 Msps is generated and demodulated by the SA.

The EVM and SNR performance of the test signal corresponding to third-order cross-modulation suppression is given in Tab. 6. As shown in Fig. 10(a), in DCM, the EVM increases with the increase of input signal power. When the input signal is lower than 6 dBm, the EVM is below the limit of 3GPP communication standard (3GPP TS 2023), whereas when the input signal is larger than 6 dBm, the EVM exceeds the limit of 3GPP communication standard (3GPP TS 2023) [35] and rises sharply due to the influence of noise such as the NLT of the VSG.

The EVM in LAM mode is significantly higher than DCM due to the gradual weakening of the PA IMD3 performance. The amplifier gradually goes into saturation when the input signal is equal to 0 dBm, at which point IMD3

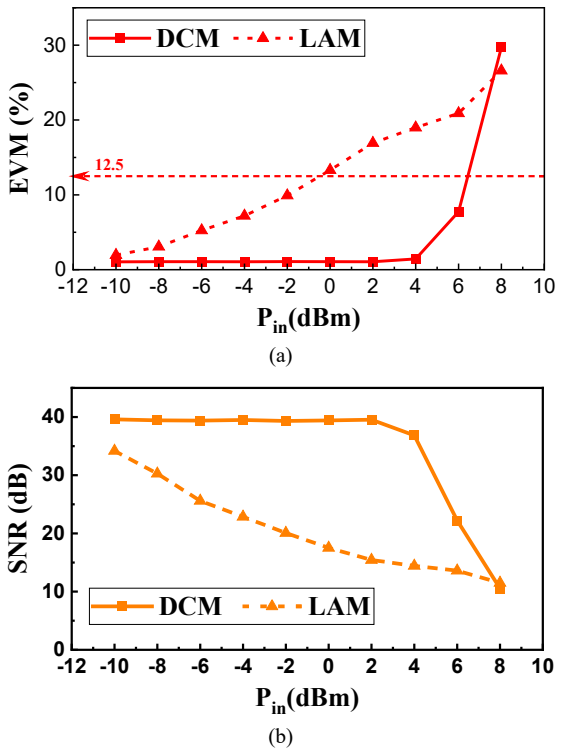

Fig. 10. Experimented 16-QAM modulation: (a) EVM and (b) SNR versus P_{in}.

reaches 15.59 dBc and EVM approaches the standard limit of 12.5%. This indicates that the signal quality deteriorates significantly, with large phase and amplitude errors, leading to more difficult symbol differentiation during demodulation and a significant increase in the bit-error-ratio (BER), which seriously affects the communication performance. When the input signal is higher than 0 dBm, the amplifier operates in the saturation region, and at this time, although the IMD3 is elevated due to the clipping effect, it introduces additional harmonic distortion and loss of dynamic range, and therefore the EVM is still rising.

By denoting PAPR the peak-to-average power ratio of the test signal after modulation, the SNR versus EVM is given by (1) [33]:

$$\mathrm{SNR}_{\mathrm{dB}} = 20\log_{10}\left(\frac{100}{\mathrm{EVM}_{\mathrm{rms}}}\right). \tag{1}$$

In the GaN HPA NLT EMI experiment on 5G TxRx communication quality, the effect of the PA on the transmission power of the communication system was measured by modulating and demodulating single carrier signal f_0 using

FSW85 SA. The signal-to-noise performance of the test signals is shown in Tab. 6. As can be seen in Fig. 10(b), in the DCM, the SNR decreases with the increase of the input signal power. When the input signal is less than or equal to 2 dBm, the SNR of 16-QAM modulation is about 40 dB, according to the approximate equation of BER (2) [33]:

$$\mathrm{BER} \approx \frac{3}{2} \cdot \mathrm{erfc}\left(\sqrt{\frac{\mathrm{SNR}_{\mathrm{linear}}}{10}}\right) \tag{2}$$

where erfc(x) is complementary error function, $\mathrm{SNR}_{\mathrm{linear}}$ is a linear representation of $\mathrm{SNR}_{\mathrm{dB}}$. At this time, the corresponding BER is almost 0, and the communication quality is excellent. When the input signal is greater than 2 dBm, the signal-to-noise ratio drops dramatically.

Similar to the performance of EVM, the SNR of LAM is lower than that of DCM; however, unlike the stable SNR level of DCM, the SNR of LAM mode shows a gradual decrease as the nonlinearity of the power amplifier increases. When IMD3 is 15.59 dBc, the SNR is 17.52 dB, and according to (2), the corresponding BER is 1.55×10^{-4}, at which time the performance of the communication link is degraded, and data transmission errors occur frequently.

3.5 Constellation Diagram Analysis

The EMI impact on the 5G communication was assessed by comparing the constellation I-Q diagram of the TxRx system in DCM and LAM. The measured constellation diagrams under 16-QAM communication for input powers $P_{\mathrm{in}} = \{-10, -4, 0, 4, 6\}$ dBm are revealed in Figs. 11. In DCM mode, the constellation points are exactly located near the symbol mapping points at $P_{\mathrm{in}} = \{-10, -4, 0, 4\}$ dBm, which indicates that the signal is stable in amplitude and phase, and less affected by noise and interference, and the modulation and demodulation process is accurate. Similar to the performance in the previous section, in LAM mode, when the input signal is 0 dBm, at which time the IMD3 is 15.59 dBc, the constellation diagram disperses significantly and begins to overshoot from square to round, which is due to amplitude compression and phase distortion caused by the nonlinear distortion, thus distorting the constellation diagram. In addition, DCM and LAM mode 64-QAM modulation EMI constellation diagram at $P_{\mathrm{in}} = \{-10, -4, 0, 4, 6\}$ dBm are plotted in Fig. 12. It can be clearly seen that the dispersion of the constellation diagrams of 64-QAM is more sensitive to the amplifier nonlinearity. Therefore, as the distortion increases, the constellation points are no longer concentrated on their respective square grids, but are distributed more randomly and tend to be circular. This indicates that it will be accompanied by higher BER and poorer communication performance.

3.6 Summary Expansion and Discussion of EMI Characterization Performance Compared to Existing Literature

In response to the above results, we make the following summaries and extensions.

QAM is a modulation method that uses both amplitude and phase to represent digital information. Nonlinearity of power amplifiers can cause distortion in both the amplitude and phase of signals simultaneously. This joint distortion of amplitude and phase can seriously affect the demodulation of signals at the receiving end. The receiving end needs to judge the transmitted digital information according to the amplitude and phase of the received signal. However, due to the distortion caused by the nonlinearity of the power amplifier, the receiving end may not be able to accurately identify the position of the signal points, resulting in an increase in the bit error rate.

Not only does the nonlinearity of the power amplifier increase the bit error rate, but it also reduces the quality of the QAM signal, manifested as a decrease in the signal-to-noise ratio and closure of the eye diagram. For example, when observing the eye diagram of a QAM signal, due to the influence of the nonlinearity of the power amplifier, the opening degree of the eye diagram will become smaller or even completely closed, which means that the margin for demodulation at the receiving end is reduced and bit errors are more likely to occur.

In addition, the nonlinearity of the power amplifier also affects the spectral efficiency of the QAM system. The QAM system achieves high spectral efficiency by transmitting more signal points within a limited bandwidth. However, the distortion caused by the nonlinearity of the power

Ref.	Communication system	EMI type	PA characteristic	Parameters discussed	Method of implementation
[34]	LTE	NL PA	-	EVM, ACLR and PAPR	Measurements and simulations
[35]	Digital modulation system (DMS) 64-QAM	NL PA	-	Constellation diagram and BER	Simulations
[36]	Digital modulation system (DMS) QPSK	Low- and high-power continuous EM wave	-	EVM and constellation diagram	Measurement
[37]	Cognitive Radio Networks	NL PA	-	SNR and ACI	Simulations
[38]	Terrestrial trunked radio	Intentional EMI	-	BER	Measurement
[39]	Multi-tone simultaneous wireless information and power transfer	NL PA	-	Symbol-error-rate	Simulations
This work	Digital modulation system (DMS) 16-QAM	NL GaN PA	Self-developed/GaN /2 GHz–6 GHz	EVM, ACLR, SNR and Constellation diagram	Measurement

Tab. 7. Performance comparison of TxRx communication EMI tests.

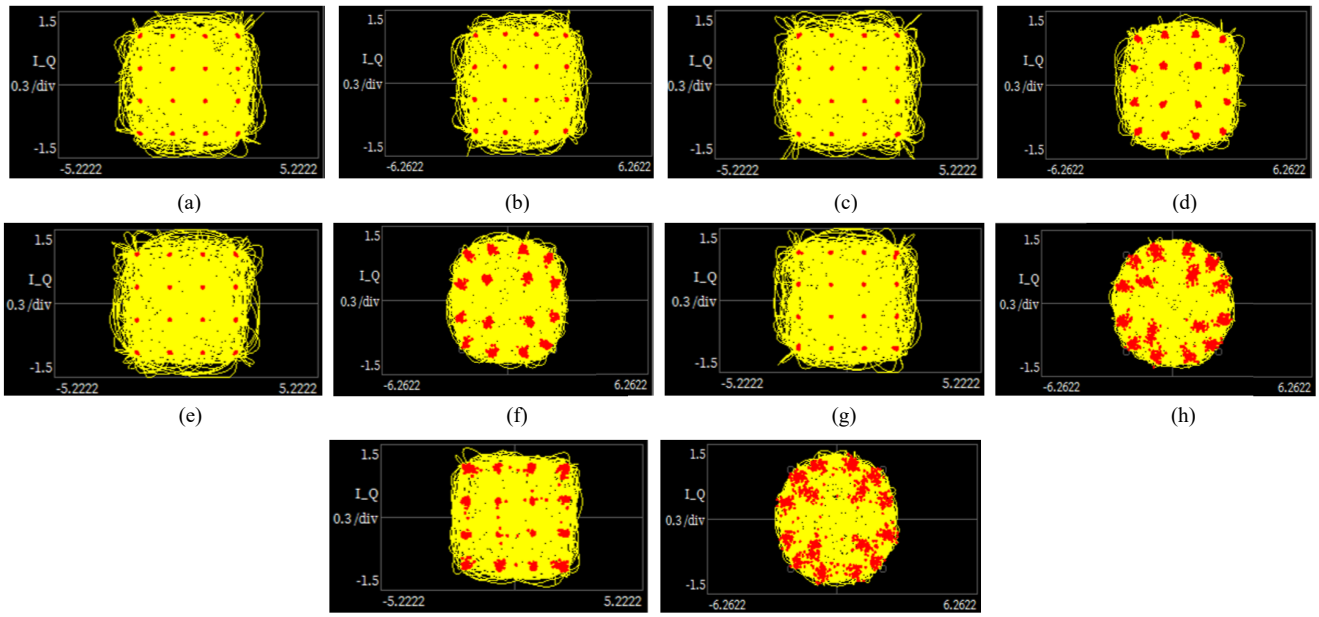

Fig. 11. Signal constellation diagram under 16-QAM modulation: in DCM: P_{in} = {(a) –10, (c) –4, (e) 0, (g) 4, (i) 6} dBm and LAM P_{in} = {(b) –10, (d) –4, (f) 0, (h) 4, (j) 6} dBm.

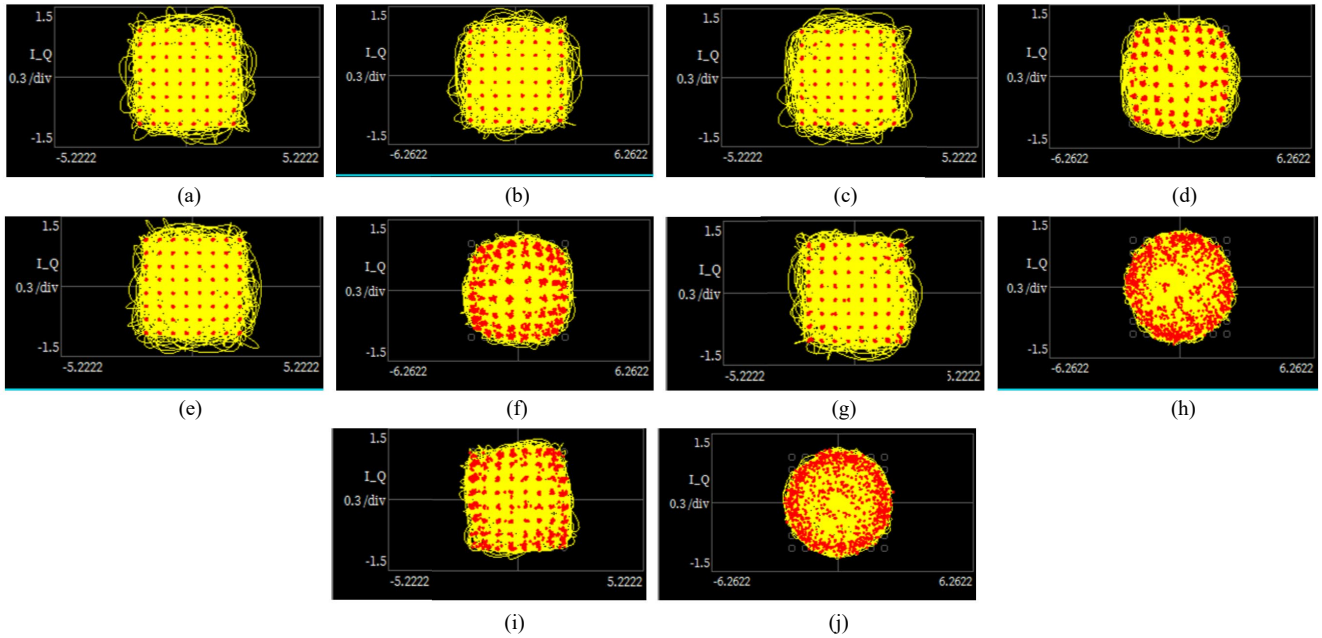

Fig. 12. Signal constellation diagram under 64-QAM modulation in DCM P_{in}={(a) –10, (c) –4, (e) 0, (g) 4, (i) 6} dBm and LAM P_{in}={(b) –10, (d) –4, (f) 0, (h) 4, (j) 6} dBm.

amplifier reduces the distinguishability between signal points, requiring more guard intervals and error correction coding, thereby reducing the actual spectral efficiency. For example, in a 64-QAM system with a theoretical spectral efficiency of up to 6 bits/Hz, due to the influence of the nonlinearity of the power amplifier, the actual spectral efficiency may only be 4–5 bits/Hz.

The EMI characterization tests developed offer considerable advantages to the EMC engineer over the existing work presented in [34–39]. Table 7 shows a quantitative comparison of the performance of EMI testing techniques. The performance of the NL effect of the TxRx element was evaluated based on the type of communication system, the type of EMI, the manufacturing process or characteristics of the amplifier, the system parameters discussed, and the study methodology.

In the context of wideband GaN amplifiers developed in-house, which are widely used in 5G communications, a testbed is constructed and the impact of the proposed GaN amplifiers on the system under digitally modulated 16-QAM

is discussed, and the performances of EVM, ACLR, SNR, and constellation diagrams are analyzed. Compared to the listed literature, the paper has significant advantages in terms of background practical urgency, self-development of broadband GaN amplifiers, parameter diversity, and simplicity of operation in higher-order modulation modes.

4. Conclusion

An experimental technique on EMI impact assessment of TxRx active components on 5G communication is investigated. The tested DUT is represented by a GaN HPA specified by 45 dB linear gain at operating frequency f_0. The NL characteristics of the HPA were elaborated from single- and double-carrier tests. The turning point of the PA input-output curve @ f_0 occurs at $P_{in} = -10$ dBm. The P1dB compression point is approximately at an input signal level of –9 dBm. Within the PA tolerance range, the maximum output power is 40.5 dBm. The IMD3 was quantified by a dual-tone input signal at carrier-frequencies f_1 and f_2, MATLAB was employed to process specific data.

With 5G communication signal operating frequency @ f_0 with 16-QAM, we state the following conclusion:

- In DCM: The EVM of various channels (signals) fluctuates within a small range. The internal demodulation reference signal shows optimized EVM and SNR. The SNR peak in the downstream channel reaches 39.6 dB. The communication quality is good in DCM. The points on the constellation diagram are accurately located near the symbol mapping points.
- In LAM: When the PA operates in the linear region, the EVM and SNR fluctuate smoothly. However, when the PA operates in the NL region and the IMD3 components becomes significant, the EVM of the signal gradually increases at a fast rate, and the SNR decreases linearly. Eventually, SNR drops below 20 dB, indicating a substantial presence of noise and interference in the communication channel. The points on the constellation diagram are affected, spreading, shifting, or deforming. The relative distance between the points and the symbol mapping points increases, leading to larger phase errors and rapid degradation in communication quality.

The developed test technique will be applicable to the next step of higher order M-QAM modulation in order to easily split the effect of GaN amplifiers on different modulation modes under the same platform and will be further discussed as an example in 5G multicarrier communication scenarios, useful for RFI analysis of 6G future communication systems. In the continuation of the present study, the EMI reduction for NL RF components will be added to the multipath channel interference based on the use of negative group delay method [40], [41].

Acknowledgments

The research was carried out within the framework of joint project with the support of the National Key Research and Development Program of China (2022YFE0122700) and the Belarusian Republican Foundation for Fundamental Research (T22KITG-018).

Statement

The data source for the results of this article can be accessed from the following link: https://dx.doi.org/10.21227/shge-2674.

References

[1] SAAD, W., BENNIS, M., CHEN, M. A vision of 6G wireless systems: Applications, trends, technologies, and open research problems. *IEEE Network*, 2020, vol. 34, no. 3, p. 134–142. DOI: 10.1109/MNET.001.1900287

[2] WIKLUNDH, K., STENUMGAARD, P. EMC challenges with 6G. In *2022 International Symposium on Electromagnetic Compatibility -EMC Europe*. Gothenburg (Sweden), 2022, p. 19–24. DOI: 10.1109/EMCEurope51680.2022.9901285

[3] WIKLUNDH, K., STENUMGAARD, P. EMC challenges for the era of massive Internet of Things. *IEEE Electromagnetic Compatibility Magazine*, 2019, vol. 8, no. 2, p. 65–74. DOI: 10.1109/MEMC.2019.8753447

[4] YAKLAF, S. K. A., TARMISSI, K. S., SHASHOA, N. A. A. 6G mobile communications systems: Requirements, specifications, challenges, applications, and technologies. In *IEEE 1st International Maghreb Meeting of the Conference on Sciences and Techniques of Automatic Control and Computer Engineering MI-STA*. Tripoli (Libya), 2021, p. 679–683. DOI: 10.1109/MI-STA52233.2021.9464470

[5] MORDACHEV, V., SINKEVICH, E., YATSKEVICH, Y., et al. Simulation of nonlinear interference in aircraft systems operating in complex electromagnetic environment created by land-based and air-based wireless systems. In *2017 International Symposium on Electromagnetic Compatibility - EMC EUROPE*. Angers (France), 2017, p. 1–6. DOI: 10.1109/EMCEurope.2017.8094819

[6] SINKEVICH, E. V. Discrete nonlinear simulation of radio receivers for electromagnetic compatibility analysis and design: Estimation of the signal-to-interference ratio. In *2007 7th International Symposium on Electromagnetic Compatibility and Electromagnetic Ecology*. St. Petersburg (Russia), 2007, p. 166–169. DOI: 10.1109/EMCECO.2007.4371677

[7] ABUELMA'ATTI, M. T. Analysis of the effect of radio frequency interference on the DC performance of bipolar operational amplifiers. *IEEE Transactions on Electromagnetic Compatibility*, 2003, vol. 45, no. 2, p. 453–458. DOI: 10.1109/TEMC.2003.811312

[8] VAN DER HORST, M. J., LINNENBANK, A. C., VAN STAVEREN, A. Amplitude-modulation detection in single-stage negative-feedback amplifiers due to interfering out-of-band signals. *IEEE Transactions on Electromagnetic Compatibility*, 2005, vol. 47, no. 1, p. 34–44. DOI: 10.1109/TEMC.2004.842116

[9] FIORI, F. A new nonlinear model of EMI-induced distortion phenomena in feedback CMOS operational amplifiers. *IEEE Transactions on Electromagnetic Compatibility*, 2002, vol. 44, no. 4, p. 495–502. DOI: 10.1109/TEMC.2002.804766

[10] YEH, M.-L., LIOU, W.-R., HSIEH, H.-P., et al. An electromagnetic interference (EMI) reduced high-efficiency switching power amplifier. *IEEE Transactions on Power Electronics,* 2010, vol. 25, no. 3, p. 710–718. DOI: 10.1109/TPEL.2009.2035622

[11] BAYRAM, Y., VOLAKIS, J. L., MYOUNG, S. K., et al. High-power EMI on RF amplifier and digital modulation schemes. *IEEE Transactions on Electromagnetic Compatibility*, 2008, vol. 50, no. 4, p. 849–860. DOI: 10.1109/TEMC.2008.2004600

[12] PARESCHI, F., ROVATTI, R., SETTI, G. EMI reduction via spread spectrum in DC/DC converters: State of the art, optimization, and tradeoffs. *IEEE Access*, 2015, vol. 3, p. 2857–2874. DOI: 10.1109/ACCESS.2015.2512383

[13] AUER, M., KARACA, T. Spread spectrum techniques for class-D audio amplifiers to reduce EMI. *Elektrotechnik und Informationstechnik*, 2016, vol. 133, p. 43–47. DOI: 10.1007/s00502-015-0384-4

[14] JIN, C., TAN, M. T., SEE, K. Y. Filterless class-D amplifier with pseudorandomized carrier frequency modulation for EMI reduction. *IEEE Transactions on Electromagnetic Compatibility*, 2013, vol. 55, no. 1, p. 74–80. DOI: 10.1109/TEMC.2012.2212907

[15] MRAD, R., PILLONNET, G., MOREL, F., et al. Predicting the impact of magnetic components used for EMI suppression on the base-band of a power amplifier. *IEEE Transactions on Power Electronics,* 2015, vol. 30, no. 8, p. 4199–4208. DOI: 10.1109/TPEL.2014.2351421

[16] FILION, B., NGUYEN, A. T., RUSCH, L. A., et al. Postcompensation of nonlinear distortions of 64-QAM signals in a semiconductor-based wavelength converter. *Journal of Lightwave Technology*, 2016, vol. 34, no. 9, p. 2127–2138. DOI: 10.1109/JLT.2016.2523680

[17] VANCAILLIE, L., KILCHYTSKA, V., ALVARADO, J., et al. Characterization and design methodology for low-distortion MOSFET-C analog structures in multithreshold deep-submicrometer SOI CMOS technologies. *IEEE Transactions on Electron Devices*, 2006, vol. 53, no. 2, p. 263–269. DOI: 10.1109/TED.2005.861725

[18] PALUMBO, G., PENNISI, S., High-frequency harmonic distortion in feedback amplifiers: Analysis and applications. *IEEE Transactions on Circuits and Systems I: Fundamental Theory and Applications*, 2003, vol. 50, no. 3, p. 328–340. DOI: 10.1109/TCSI.2003.808835

[19] MAFFEZZONI, P. Efficient multiparameter sensitivity computation of amplifier harmonic distortion. *IEEE Transactions on Circuits and Systems II: Express Briefs*, 2007, vol. 54, no. 3, p. 257–261. DOI: 10.1109/TCSII.2006.888725

[20] MIAO, Y., ZHANG, Y. Distortion modeling of feedback two-stage amplifier compensated with Miller capacitor and nulling resistor. *Transactions on Circuits and Systems I: Regular Papers,* 2012, vol. 59, no. 1, p. 93–105. DOI: 10.1109/TCSI.2011.2161393

[21] SHI, G. Symbolic distortion analysis of multistage amplifiers. *IEEE Transactions on Circuits and Systems I: Regular Papers*, 2019, vol. 66, no. 1, p. 369–382. DOI: 10.1109/TCSI.2018.2859242

[22] BAXEVANAKIS, D., SOTIRIADIS, P. P. A general time-domain method for harmonic distortion estimation in CMOS circuits. *IEEE Transactions on Computer-Aided Design of Integrated Circuits and Systems*, 2021, vol. 40, no. 1, p. 157–170. DOI: 10.1109/TCAD.2020.2988414

[23] CELIK, A., ZHANG, Z., SOTIRIADIS, P. P. A state-space approach to intermodulation distortion estimation in fully balanced bandpass Gm-C filters with weak nonlinearities. *IEEE Transactions on Circuits and Systems I: Regular Papers*, 2007, vol. 54, no. 4, p. 829–844. DOI: 10.1109/TCSI.2006.887630

[24] PINI, G., MANSTRETTA, D., CASTELLO, R. Analysis and design of a 20-MHz bandwidth, 50.5-dBm OOB-IIP3, and 5.4-mW TIA for SAW-less receivers. *IEEE Journal of Solid-State Circuits*, 2018, vol. 53, no. 5, p. 1468–1480. DOI: 10.1109/JSSC.2018.2791489

[25] XIAO, Z., JING, X., A novel characteristic parameter approach for analysis and design of linear components in nonlinear systems. *IEEE Transactions on Signal Processing*, 2016, vol. 64, no. 10, p. 2528–2540. DOI: 10.1109/TSP.2016.2526967

[26] FIORI, F. EMI-induced distortion of baseband signals in current feedback instrumentation amplifiers. *IEEE Transactions on Electromagnetic Compatibility*, 2018, vol. 60, no. 3, p. 605–612. DOI: 10.1109/TEMC.2017.2736537

[27] FIORI, F. L., CROVETTI, P. S. Prediction of high-power EMI effects in CMOS operational amplifiers. *IEEE Transactions on Electromagnetic Compatibility*, 2006, vol. 48, no. 1, p. 153–160. DOI: 10.1109/TEMC.2006.870690

[28] GOLUBOVICH, D., CHERMOSHENTSEV, S. Virtual testing of the emission of electromagnetic interference from electronic means according to the electromagnetic compatibility requirements. In *2019 International Conference on Electrotechnical Complexes and Systems (ICOECS)*. Ufa (Russia), 2019, p. 1–4. DOI: 10.1109/ICOECS46375.2019.8950005

[29] PARVIS, M., PERRONE, G., VALLAN, A. A precompliance EMC test-set based on a sampling oscilloscope. *IEEE Transactions on Instrumentation and Measurement,* 2003, vol. 54, no. 4, p. 1220 to 1223. DOI: 10.1109/TIM.2003.816839

[30] MORDACHEV, V., SINKEVICH, E. Experimental analysis of radio receiver susceptibility to out-of-band interference by means of double-frequency test system. In *10th International Symposium on Electromagnetic Compatibility*. York (UK), 2011, p. 405–411.

[31] SINKEVICH, E., MORDACHEV, V. Investigation of the transmitter susceptibility to reverse intermodulation by the use of double-frequency diagrams. In *2015 IEEE International Symposium on Electromagnetic Compatibility (EMC)*. Dresden (Germany), 2015, p. 1159–1164. DOI: 10.1109/ISEMC.2015.7256333

[32] 3GPP TS 38.104 V18.3.0. 3rd generation partnership project; technical specification group radio access network, NR, base station (BS) radio transmission and reception (Release 18). *3rd Generation Partnership Project* (3GPP). Sep. 2023.

[33] PROAKIS, J. G. *Digital Communications.* 4th ed. New York (USA): McGraw-Hill, 2001. ISBN: 978-0071181839

[34] JOVANOVIC, B., MILENKOVIC, S. Transmitter IQ imbalance mitigation and PA linearization in software defined radios. *Radioengineering*, 2022, vol. 31, no. 1, p. 144–154. DOI: 10.13164/re.2022.0144

[35] CHEN, S., HONG, X., KHALAF, E., et al. Adaptive B-spline neural network based nonlinear equalization for high-order QAM systems with nonlinear transmit high power amplifier. *Digital Signal Processing*, 2015, vol. 40, p. 238–249. DOI: 10.1016/j.dsp.2015.02.006

[36] DUBOIS, T., LAURIN, J.-J., RAOULT, J., et al. Effect of low and high power continuous wave electromagnetic interference on a microwave oscillator system: From VCO to PLL to QPSK receiver. *IEEE Transactions on Electromagnetic Compatibility*, 2014, vol. 56, no. 2, p. 286–293. DOI: 10.1109/TEMC.2013.2280670

[37] MAJIDI, M., MOHAMMADI, A., ABDIPOUR, A. Analysis of the power amplifier nonlinearity on the power allocation in cognitive radio networks. *IEEE Transactions on Communications*, 2014, vol. 62, no. 2, p. 467–477. DOI: 10.1109/TCOMM.2014.011114.130094

[38] VAN DE BEEK, S., LEFERINK, F. Robustness of a TETRA base station receiver against intentional EMI. *IEEE Transactions on Electromagnetic Compatibility*, 2015, vol. 57, no. 3, p. 461–469. DOI: 10.1109/TEMC.2015.2406732

[39] PARK, J. J., MOON, J. H., JANG, H. H., et al. Performance analysis of power amplifier nonlinearity on multi-tone SWIPT. *IEEE Wireless Communications Letters*, 2021, vol. 10, no. 4, p. 765–769. DOI: 10.1109/LWC.2020.3042852

[40] RAVELO, B., WAN, F., NEBHEN, J., et al. Resonance effect reduction with bandpass negative group delay fully passive function. *IEEE Transactions on Circuits and Systems II: Express Briefs*, 2021, vol. 68, no. 7, p. 2364–2368. DOI: 10.1109/TCSII.2021.3059813

[41] RAVELO, B., LALLÉCHÈRE, S., RAHAJANDRAIBE, W., et al. Electromagnetic cavity resonance equalization with bandpass negative group delay. *IEEE Transactions on Electromagnetic Compatibility*, 2021, vol. 63, no. 4, p. 1248-1257. DOI: 10.1109/TEMC.2021.3051100

[42] DU, H. *GaN Power Amplifier Nonlinear Test Results*. [Online] Accessed 2024-09-18. Available at: https://dx.doi.org/10.21227/shge-2674

About the Authors …

Hongyu DU was born in China. She received the B.Eng. degree in Communication Engineering in 2018 from the Nanjing University of Information Science and Technology, Nanjing, China, where she is currently working toward the Ph.D. degree. Her research interests include negative group delay mechanism and complex permittivity measurement technology.

Fayu WAN (corresponding author) was born in China. He received the Ph.D. degree in Electronic Engineering from the University of Rouen, Rouen, France, in 2011. From 2011 to 2013, he was a Postdoctoral Fellow with the Electromagnetic Compatibility Laboratory, Missouri University of Science and Technology, Rolla, MO, USA. He is currently a Full Professor with the Nanjing University of Information Science and Technology, Nanjing, China. His research interests include negative group delay circuits, electrostatic discharge, electromagnetic compatibility, and advanced RF measurement.

Vladimir MORDACHEV was born in in Vitebsk, Belarus. He received the M.S. degree (with honors) and the Ph.D. degree in Radio Engineering from the Minsk Radio Engineering Institute, Minsk, Belarus, in 1974 and 1984, respectively. He received an academic rank of Senior Scientist in 1985. His current research interests include spectrum management, wireless communications and networks, electromagnetic compatibility and interference, wireless network planning, computer-aided analysis and design, cellular networks system ecology, RF systems modeling, and simulation. He is extensively involved in consulting to wireless network operators, industry and the local government. He is the Head of the Electromagnetic Compatibility Laboratory, Belarusian State University of Informatics and Radioelectronics, Minsk, Belarus.

Eugene SINKEVICH received the M.S. degree in Radio System Engineering (summa cum laude) from the Belarusian State University of Informatics and Radioelectronics (BSUIR), Minsk, Belarus, in 2000. From 2000 to 2003, he was with the Department of Radio Engineering Theory, BSUIR. From 2004 to 2005, he was with the Department of Radio Devices, BSUIR. Since 2005, he is with the EMC R&D Laboratory, BSUIR, where he is currently the Senior Researcher, Team Leader, and Principal Designer of International R&D projects. His current research interests include electromagnetic compatibility, RF and microwave measurements, and wireless systems and devices. He is the author of about 20 technical papers in international journals and conference proceedings.

Xiaohe CHEN received the Ph.D. degree from Missouri University of Science and Technology in 2007. Since 2007, he has been working as a director system architect in the Design Analysis and Product Blueprinting Department at Apple HQ. In 2015, he has been working as the director of the Electromagnetic Compatibility Research Center of Suzhou Institute of Biomedical Engineering and Technology, Chinese Academy of Sciences, and the director of the Research Laboratory of Medical Electronics; and he will be a professor and a doctoral director at the School of Informatics, China University of Petroleum, China, in 2022. His research interests are biomedical informatics, artificial intelligence, signal processing, signal integrity research, electromagnetic compatibility.

Blaise RAVELO is currently a University Full Professor with the Nanjing University of Information Science and Technology, Nanjing, China. He supervised ten Ph.D. students. He has coauthored more than 430 scientific research papers in new technologies published in international conference and journals. His research interests include multiphysics modeling, Kron's method, RF/electronics engineering, EMC/SI/PI of PCBs, and pioneer of the negative group delay theory, engineering and application for data prediction. With international partners, he is actively involved and contributes on several international research projects. He is a Member of IET. He is an Associate Editor and the Circuit and System Subject Editor of the Editorial Board of IET Electronics Letters. He is a Member of Scientific Technical Committee of International Conference on Antennas and Electromagnetic Systems. He is ranked in Top 2% world's scientists based on years (during 2020–2024) by Stanford University, U.S. He has Google scholar H-index(2024) = 31 and i10-index(2024) = 113. He is a member of research groups: URSI, GDR Ondes, Radio Society.